SECONDARY ANCHOR TARGETED CELL RELEASE SYSTEM

BY

ALI ANSARI

THESIS

Submitted in partial fulfillment of the requirements
for the degree of Master of Science in Bioengineering
in the Graduate College of the
University of Illinois at Urbana-Champaign, 2016

Urbana, Illinois

Advisor:

Professor Princess I. Imoukhuede

ABSTRACT

The lack of diagnostic tools that can probe individual heterogeneities in patient's cell receptor expression limits advancement in personalized medicine. These individual differences in receptor quantities can give rise to both intrinsic and acquired resistances to therapeutics, which result in reduced treatment efficacy. In diseases like cancer, where therapeutics have many adverse side effects, noting which drugs have reduced efficacy means the difference between remission and death.

Current chemical and physical cell separation methodologies may result in disruption of physiological receptor quantities. These changes in receptor quantities and expression may hide changes that give diagnostic information about tumor progression and environment. Thus separation techniques which hide these changes in receptor expression would be sub-optimal diagnostic tools. Here we describe a functionalization process that facilitates gentle cell capture with subsequent cell release via a secondary, surface-anchoring mechanism. The cellular capture system consists of glass functionalized with APTES, d-desthiobiotin and streptavidin, which when coupled with biotinylated antibodies, such as mCD11b and hIgG, are used to capture mouse macrophages (RAW 264.7) and human breast cancer (MCF7-GFP) cell lines, respectively. Cell release is facilitated through the introduction of biotin, allowing for the enrichment of the cells of interest captured by the surface. This release is done through the targeting of the secondary moiety desthiobiotin, which results in a much more gentle release paradigm. This reduction in harsh reagents and shear forces reduces changes in cellular expression. The functionalized surface captures up to 80% of cells in a single cell mixture and has demonstrated 50% capture in a dual-cell mixture. This engineering advancement is a critical step towards achieving cell isolation platforms for personalized medicine.

ACKNOWLEDGEMENTS

I would like to thank the American Cancer Society, Illinois Division (282802), the National Science Foundation CBET (1512598), and Mexico's National Council of Science and Technology (CONACyT) for funding support. I also would like to thank both Scott Maclaren and Dr. Dianwen Zhang from the University of Illinois Fredrich Seitz Material Research Laboratory and Beckman Institute for AFM and microscopy training. Finally, I would like to thank my family, Dr. Imoukhuede, Dr. Kris Kilian, Jared Weddell, Stacie Chen, Spencer Mamer, and Ritu Raman for insightful discussions, as well as the tremendous assistance in research and life, without which I could not have gotten this far.

TABLE OF CONTENTS

CHAPTER 1
INTRODUCTION

1.1 Motivation

Many leading cancer research foundations (e.g., ACS, NCI, AACR) have identified the critical need for more personalized treatments and medicines in the advancement of cancer therapies[1–3]. Personalized medicine is critical as it allows the customization of treatment regimens to patients based on their distribution of cell-surface receptors on specific cells within a tissue[4]. Patient cell-surface receptors expression levels can contribute very strongly to both drug and therapy resistances[5], implying that receptor level profiling would allow greater personalization for treatments. Indeed, by applying quantitative flow (qFlow) cytometry[6], we recently showed that variability in cell-surface vascular endothelial growth factors can mathematically define tumor endothelial cell subpopulations from breast cancer xenografts[7]. We computationally predicted how these tumor-associated cell sub-populations would elicit differing Avastin, therapeutic response[8]—accordingly, isolating and profiling tumor and tumor-associated cells could offer a new approach for personalized prediction of Avastin and other anti-angiogenic therapeutic responsiveness[8]. In order to begin profiling these cellular receptors to target and personalize treatments, there is a distinct need for cellular isolation systems that can isolate samples rapidly and efficiently, while preserving cell-surface receptor-levels.

This thesis is focused on the development and integration of a novel secondary anchor targeted cell release system that operates through the functionalization of several layers of proteins and materials on glass surfaces. The tuning and optimization of this surface for a variety of cell types and modalities would allow for the application of this technology beyond the scope of just cancer

and cardiovascular diseases, allowing for any enrichment of rare cell types for the diagnosis of disease.

1.2 Overview

The thesis is separated into chapters that will allow for better understanding of cellular isolation and its significance. Chapter 2 discusses what the Secondary Anchor targeted Cell Release system consists of as well as why it is important. We also discuss the functionalization process and its applications. Chapter 3 will first describe customization of the functionalization of the surface. It will then expand on the integration and future aims of this technology into a clinically translated microfluidic devices for personalized care.

CHAPTER 2

SECONDARY ANCHOR TARGETED CELL RELEASE[1]

2.1 Introduction

In order to achieve the promise of personalized medicine profiling, systems are needed that can quickly, and efficiently isolate specific cell types without disrupting cell-surface receptor-levels. The "lab on a chip" concept offers the promise of >100X faster (hours-to-minutes) cell isolation. Some approaches novel approaches include optical trapping[9,10], microfluidics[11–13], and surface functionalization[14–16]. While, these approaches offer the advantages of sensing protein[17,18] or RNA expression[19–21] or providing cells for in vitro culture[16,22], many cannot be applied towards the quantitative profiling of cell-surface receptors, because they cause irreversible damage to cells. Indeed, fluid shear forces, as low as 0.5–5 Pa, can trigger necrosis or cell fracture[23] and mild chemical digestion (e.g., collagenases, trypsin) can cleave cell-surface receptors[24,25], while cell lysis renders cell-surface receptors indistinguishable from intracellular receptors[26]. New methods are therefore needed to capture and release endothelial cells while preserving cell surface-receptor levels.

Here we present a new method of secondary anchor targeted cell release that should preserve cell structure and function. The primary anchor, a biotinylated antibody, binds to cells and the

---

[1]This work has been been previously published by the degree candidate

Citation information: Ansari, A., Lee-Montiel, F. T., Amos, J. R. and Imoukhuede, P. I. (2015), Secondary anchor targeted cell release. Biotechnol. Bioeng., 112: 2214–2227. doi:10.1002/bit.25648

secondary anchor, a streptavidin (SAv) – d-desthiobiotin (DSB) (reversible) -functionalized surface, is targeted for cell release through biotin competition ($K_{d\ desthiobiotin\text{-}streptavidin} = 10^{-13}$, $K_{d,biotin\text{-}streptavidin} = 10^{-15}$)[27–29]. DSB is a biotin analogue that differs from biotin in that it lacks one sulfur group, resulting in a 100-fold decrease in its affinity for SAv and is easily displaced by biotin. The interaction between DSB and SAv is used to pull-down cells, and the competing interaction of excess biotin replaces the DSB, resulting in the passive release of the capture surface without additional force.

We identify optimal conditions for surface functionalization by varying and analyzing surface properties. We demonstrate SAv-Quantum dots (SAv-Qdots) capture and release, MCF7-GFP capture and release, and selective capture and release of RAW 264.7 (mouse macrophage cell line) from a dual-cell mixture. This new method provides an effective cell capture and release that can be applied to isolate target cells from multi-cells samples.

2.2 Materials and Methods

Concept. The cellular capture system consists of a functionalized glass surface involving four major layers: (3-Aminopropyl) triethoxysilane (APTES); DSB (for reversible binding to SAv); SAv; and a cell-specific biotinylated antibody (Fig. 1). The cells are captured by the antibodies on this surface and released via introduction of excess biotin, which competes with the DSB.

Surface functionalization. Several glass surfaces were used: an uncoated 8-well culture slide (BD Falcon, San Jose, California), plain microscope slides (Corning, Catalog number 2947-75X38, Tewksbury, MA), microscope cover slides (Thermo Scientific, Catalog Number 22X70, Waltham, MA), Lab-Tek II 8-well slides (Nunc / Thermo Scientific, Catalog Number 154534,

Pittsburgh, PA), and Glass bottom P24G-0-13-F, 24-well plates (MatTek, Ashland, MA). Glass was cleaned using Diener Plasma Cleaner Pico (Royal Oak, MI) for 5 min at 50% power. 2% (3-Aminopropyl) triethoxysilane (APTES) (Acros Organics, Geel, Belgium) in ethanol was applied to the oxygen plasma cleaned glass surface for 50 min and cured in a Thermo Scientific Precision Oven (Thermo Scientific, Pittsburg, PA) for 2 h at 55°C. d-Desthiobiotin (DSB) (Sigma, St. Louis, MO) was solubilized with 10 µL dimethyl sulfoxide (BDH, Radnor, PA) per mg of DSB. The DSB carbonyl group at 1.5 mg/mL was activated and combined with 1-Ethyl-3-(3-dimethylaminopropyl) carbodiimide (EDC) (Thermo Scientific, Pittsburg, PA). The activated DSB was dissolved in pH 6.0, 2-(N-morpholino) ethanesulfonic acid (MES buffer) for 15 min and quenched using mercaptoethanol. Following overnight incubation at 4°C in a refrigerator, excess DSB was washed with phosphate buffered saline (PBS) three times and 0.4 mg/mL streptavidin (Proteochem, Loves Park, IL) in PBS was applied overnight at 4°C, rinsed with PBS, rewetted, and replaced in the refrigerator until use. This functionalization protocol was adapted and modified from existing literature[30].

Cell culture. MCF7-GFP cells, a luminal breast cancer cell line, were obtained from Cell Biolabs (San Diego, CA). MCF7-GFP cells were grown in high glucose Dulbecco's modified Eagle medium (DMEM) supplemented with nonessential amino acids (University of Illinois Cell Media Facility, School of Chemical Sciences, Urbana, IL), 10% fetal bovine serum (Invitrogen, Carlsbad, CA), and 1% Penicillin–Streptomycin (Invitrogen). The RAW 264.7 mouse macrophages were gifted to us from the Smith lab at the University of Illinois. RAW 264.7 cells were grown in DMEM containing 10% fetal bovine serum and 1% penicillin-streptomycin. All cells were maintained at 37°C in 95% air, 5% CO_2. Cells were grown to confluence before the

experiment. For routine cell passaging, cells were detached from flasks using TrypLe (Life Technologies, Carlsbad, CA). For capture experiments, CellStripper cell dissociation solution (Corning, Manassas, VA) was applied for 5–7 min at 37°C. Cells were re-suspended in 10 mL stain buffer, which contains from PBS with 1% BSA and 0.09% sodium azide. Cells were centrifuged at 500 x g for 5 min at 4°C, the supernatant aspirated, and cells re-suspended in cold Hanks Balanced Salt Solution without calcium, magnesium, or phenol red to a final concentration of $1x10^6$ cells/mL.

Antibody biotinylation. Antibodies were biotinylated at a concentration of 0.5 mg hIgG/mL or 1 mg mCD11b/mL using the EZ-Link Sulfo-NHS-LC Biotinylation Kit (Thermo-Scientific, Waltham, MA), following the manufacturer's instructions. Briefly, antibody was incubated with Sulfo-NHS linked biotin for two hours. Biotinylated antibody was purified with Zeba Spin Desalting columns (Thermo Scientific, Waltham, MA) and centrifuged at 1000x g for 2 min. For small-volume samples, a stacker was applied, ensuring complete sample flow through the desalting column.

Cell capture. MCF7-GFP cells were targeted with either by hIgG, HP6017 (BioLegend, San Diego, CA) or hHLA-A,B,C, 311402 (BioLegend, San Diego, CA) and RAW 264.7 cells were targeted with mCD11b, MA5-17826 (Thermo Scientific). The antibodies and the cells were incubated for 30 min at 4°C in an end-over-end mixer. The functionalized glass surfaces were uncoated 8-well plates that were initially washed with Hank's Balanced Salt Solution without calcium and without magnesium (HBSS) before incubation of cells. 300 µL of cells concentrated to one million cells/mL (300,000 cells) were seeded in each well. Cells were incubated for 45

min on ice on a shaker. Following cell capture, surfaces were gently washed with 500 µL HBSS and resuspended in 200 µL HBSS (control) or released with 300 µL of 20 mM biotin (Amresco, Solon, OH). After a 20 min shaking on ice, all wells were gently washed with HBSS 500 µL HBSS and resuspended in 200 µL HBSS.

Fluorescence Microscopy. SAv- Qdots were seeded in a functionalized 8-well coverglass (Thermo Labtek II) and incubated for 45 min at 25 °C to allow for SAv-Qdot-DSB attachment. Qdots were imaged on an inverted Zeiss LSM 710 Confocal Microscope at 8 bits using 5 channels and 512 x 512 pixel resolution. Cells were excited with a 405 nm laser at 17%–22% laser power using a 63x apochromat 1.4 NA oil-immersion objective. Fluorescence was collected with the 32-channel Quasar multichannel photomultiplier tube. Wide-Field cell imaging was performed on a Zeiss Axiovert 200 M inverted florescence microscope in the Beckman Institute at the University of Illinois at Urbana-Champaign, using a 10x Plan-Neofluar objective with a numerical aperture of 0.30 and a working distance of 5.6 mm in air. The Axiovert uses a 120 Hg UV lamp and imaged GFP fluorescence using the 470EX/515EM FITC Chroma Set 41025. Images were analyzed using the FIJI, Image J software package.

Atomic force microscopy. All AFM measurements were performed in tapping mode on an Asylum Research MFP-3D AFM (Asylum Research, Santa Barbara, CA). The scan rate was 1Hz, and 256 line resolution. The scan size was 1x1 µm. The scanning angle was 90°, the drive amplitude was 0.3166 to 0.37704, and the Drive frequency was 310,000. We used Tap300-G silicon tips from Budget Sensors (Sofia, Bulgaria) with a force constant of 40 N/m. Igor

(WaveMetrics, Portland, OR) was used to analyze the raw AFM data and obtain the standard deviation data.

Antibody and cell titration studies. 24-well plates (MatTek) were functionalized and then titrated across several different concentrations of cells and antibodies to find the optimum concentrations for both. For the antibody titration, five different concentrations of HLA-ABC antibodies, ranging from 1-10,000 ng/mL were used. MCF7-GFP cells at $1x10^6$ million cells/mL were incubated on the surface for 45 min and gently washed any non-adherent cells. The 24-well plates were imaged on a Biotek Synergy HT Plate Reader (Biotek, Winooski, VT) at 485nm, 528 nm emission. Data were analyzed with OriginLab (Origin Corp, Northampton, MA) to determine the optimum antibody concentration of 10 ng/mL. We used the optimum concentration for cell titration, adding 10 ng/mL HLA-ABC or hIgG antibody to six different concentrations of MCF7-GFP cells, ranging from 10-1,000,000 cells/mL. After a 45 min incubation, we gently washed any non-adherent cells and imaged MCF7-GFP fluorescence with the plate reader.

2.3 Results

Testing uniformity of SAv functionalization. To identify SAv concentrations and incubation times leading to optimal capture and uniformity, we imaged the Labtek II glass surface functionalized with APTES, DSB, and SAv; incubated with biotinylated-Qdots 605; and performed wide-field fluorescence imaging. The 0.3 mg/mL SAv functionalization showed the lowest fluorescence intensity (Figs. 2A and 2B), suggesting that this lower SAv concentration did not enable optimal capture. Furthermore, we observed a large standard deviation in the

fluorescence intensity, indicating non-uniform surface binding. 0.5 mg/mL SAv functionalization resulted in the highest Qdot fluorescence intensity, which indicates high-capture onto the surface. However, this condition also had the highest fluorescence standard deviation, indicating regions of aggregation rather than uniform surface coverage. The 0.4 mg/mL SAv functionalization displayed ~20% lower fluorescence intensity relative to the 0.5 mg/mL case; it gave greater uniformity in Qdot coverage compared to either 0.3 mg/mL or 0.5 mg/mL as calculated via a standard deviation in fluorescence coverage. Additionally, we tested SAv incubation time, which showed that overnight incubation (18-20 h) resulted in 80% higher SAv-Qdots binding compared to 4 h incubation (Fig. 2C), indicating that cellular capture before overnight incubation was not optimized (Supplementary Fig. 1). Thus, the 0.4 mg/mL, incubated overnight SAv enabled both increased and uniform binding.

Characterizing functionalized surface uniformity. The glass cleaned with ethanol and DI water had a surface height standard deviation of 1.969 nm, which was 83% greater than the standard deviation of the glass cleaned with oxygen plasma (Table 1). Since the oxygen plasma cleaning resulted in a more uniform glass surface, we used this to treat all subsequently tested layers. The 2% APTES surface had a 7% lower standard deviation than the 5% APTES surface, indicating that the 5% APTES surface was marginally more uniform than the 2% APTES surface. However, this trend was reversed in the comparison of fully functionalized 2% APTES, DSB, and SAv functionalized surface compared to the 5% APTES, DSB, and SAv functionalized surface. In the 2% fully functionalized surface, the standard deviation was 57% lower than the standard deviation for the 5% surface. Therefore, the 5% APTES fully functionalized surface

was extremely non-uniform and not suitable as the basis of the capture surface. The 2% APTES fully functionalized surface was more uniform and thus became the basis for our capture surface.

Characterizing functionalized surface height. The functionalization of each layer affects subsequent layers, so significant variations can detrimentally affect cellular capture. We used atomic force microscopy (AFM) to image both a "dirty" (not-cleaned; Fig. 3A), and oxygen-plasma cleaned (Fig. 3B) glass surfaces modified with APTES. The dirty glass presented several non-homogenous regions (Fig. 3A), whereas, there was greater uniformity in the oxygen-plasma cleaned surface (Fig. 3B). When we examined the method of cleaning, we saw that cleaning with oxygen-plasma (Fig. 8B) had 2.5 nm less total height variation (from 3 nm to -2 nm), compared to ethanol and water surface cleaning (from 3.5 nm to 0 nm; Fig. 3A and 8A). AFM imaging of the complete, functionalized surface showed a higher range of surface height when 5% APTES (Fig. 3F and 8F) was used, with surface heights ranging from -4 to 7 nm, compared with surface heights from 6 to -2 nm with 2% APTES (Fig. 3E and 8E). Altogether, our AFM imaging showed that oxygen-plasma cleaning followed by 2% APTES functionalization provided a more uniform surface.

Calculating shear force on a SAv bond. To determine whether our washing step could disrupt the DSB-SAv or the biotin-SAv bonds, we calculated the shear force that washing applied to these bonds. It was necessary to make several assumptions for this calculation. First, we assumed that the washing occurred as a one-dimensional flow parallel to the plate surface (Fig. 9). Initially, there was 1 mL of fluid within the well, the bottom of the well has an area of 0.7 cm^2, and the washing step took approximately 2 seconds. This gave a volumetric flow rate of 0.5 mL/s

within the well with a new fluid depth of 1.4 cm. Thus, the average fluid velocity across the glass plate/liquid interface was 0.42 cm/s. The shear stress was calculated at the wall by:

$$\tau = \mu \frac{dv}{dy}\Big|_{y=0} \quad (1)$$

where τ is the shear stress at the wall, μ is the fluid viscosity, v is the fluid velocity, and y is the distance from the wall. We assumed the fluid viscosity is the same as water (μ = 1 N·s/m^2), that our average velocity occurred at the center of the fluid flow (dy = h/2 = 0.7 cm), and that there were no slip conditions along the bottom of the well plate (dv = 0.42 cm/s). This gives a shear stress at the plate interface of 0.6 N/m^2. Assuming SAv is a sphere with a diameter of 5 nm[31], the SAv surface area was 79 nm^2. We further assumed that only the top half of SAv was exposed to fluid shear stress, making the available SAv surface area 39.5 nm^2. Thus, we estimated that a single SAv bond experienced 24 x 10^{-6} pN of shear force. Prior research has shown that the force required to disrupt a biotin-avidin binding is 173 pN[32]. While data on DSB-SAv disruption forces are not available, we predict that the disruption force would be in the 84-104 pN range, given the that DSB-avidin coupling can be disrupted by forces of nearly half that of biotin-avidin[32]. Overall, these calculations indicate that the wash steps in the experiment were unlikely to shear either the SAv and DSB bond or the SAv and biotin bond.

Capture and release – Cells & Qdots: We examined the feasibility of biotin-mediated release by imaging SAv-Qdots 605 incubated on the functionalized surface (Fig. 2). We observed capture (Fig. 2A) and release via 20 min incubation with 20 mM biotin. When we extended this analysis to cells, we observed that biotinylated hIgG-bound to human MCF7-GFP cells were captured by our surface (Fig. 5A), resulting in 60% cell pull-down. When exposed to a controlled

wash to eliminate non-specific adhesion, 50% of the cells were retained on the capture surface. The non-functionalized glass surfaces resulted in 70% pull down of cells but the binding was nearly all-nonspecific as after a controlled wash, only 15% of the cells remained. This indicates an effective capture surface. 20 min 20 mM biotin treatment released ~80% of captured MCF7-GFP cells, whereas HBSS wash treatment released only 60% of attached cells.

Capture and release – Cells within a mixture: We examined the ability of the surface and antibodies to isolate target cells by introducing a dual-cell population containing human breast cancer cells (MCF7-GFP) and mouse macrophages (RAW 264.7), and we used mCD11b, an antibody specific to the mouse macrophages, to selectively capture the macrophages. We chose these cell-types (primary tumor and immune) because they represent prevalent cells types in tumor biopsies[33,34] and murine xenograft models[35]. Therefore, selective capture would be useful for future applications of this technology. Additionally, the fluorescent MCF7-GFP allowed cells to be readily imaged. We observed some non-specific adhesion of MCF7-GFP cells in the unwashed control system as indicated by the fluorescent signal (Fig. 6A) corresponding to 50% cell capture on the surface. However, this non-specific MCF7-GFP adhesion was decreased by 80% when the cells were washed with HBSS. The CD11b facilitates the binding of macrophages, as shown by the merged bright field and widefield microscopy imaging, showing non-fluorescent cells (Fig. 6). There was an ~80% decrease in the cell capture following 20 min 20 mM biotin incubation. While these results indicate effective cell capture and cell release via the biotin mechanism, the HBSS-mediated cell release suggests antibody tethering may not be highly specific.

2.4 Discussion

Cell separation facilitates the study of structure-function relationships in neuroscience[36], stem cell programming in regenerative biology, and angiogenic signaling in vascular biology[37]. However, current cell separation methods can damage cell structure. Systems are needed that can quickly and efficiently isolate specific cell types without disrupting cell-surface receptor levels. To meet these cell isolation challenges we have advanced a new methods in surface functionalization, which (1) creates a system of reliable capture of a single cell type from a mixture of cell types; (2) allows for the gentle and reproducible release of cells; and (3) raises the possibility of capturing different cell types in stages using specific antibodies.

SAv layer optimization: Surface uniformity is vital to the functionalization of the surface, as non-uniformity results in a decrease in the capture efficiency of the overall surface. In order to improve the surface uniformity, we optimized the concentration of APTES as well as the concentration of DSB. The 0.3 mg/mL and 0.5 mg/mL concentrations of SAv resulted in large amounts of non-uniformity across the surface of the glass. We chose 0.4 mg/mL as it had the lowest non-uniformity of the concentrations tested. Other concentrations of SAv have been used for surface functionalization. While this concentration is optimal for our application, there is not a consensus as to which concentration is the optimum for maximum uniformity. Indeed, prior SAv functionalization studies have used concentrations ranging from 5 μg/mL – 10 mg/mL[38–44].

AFM measurement of functionalized surface height: AFM provides a useful tool for characterizing surfaces[45–49]. In this study, AFM provided insights into both the absolute height of the functionalized surfaces and the surface functionalization variability. When we compared these heights to prior surface functionalization, we observed that the APTES functionalization

was within the ellipsometry measured range of 5.2 ± 1.8 nm and the 2% APTES, DSB, and SAv was well within 9.7 ± 4.4 nm[49]. In addition to height data, we used standard deviation to judge uniformity of the surface. We found that 2% APTES full functionalization produced the least variability in height. These metrics have been used by others to successfully identify surface variation in a variety of materials including orthodontics[50], thin films[51], nanofiltration membranes[52] and dentin[53]. We concluded that the 2% APTES fully functionalized was the more uniform surface as it had a lower degree of surface roughness.

Applications of AFM: While there are several approaches for AFM-mediated surface imaging (e.g., contact-mode, near contact mode, affinity imaging, etc.), we applied tapping mode for this study, in which, a consistent oscillation directs the tip to tap the surface. Tapping mode imaging is advantageous because it combines near contact and accuracy of reading, without the destructiveness or tip-induced artifacts that can occur when imaging soft materials[54]. In addition to our application of tapping AFM to height measurements and uniformity, AFM has successfully been applied towards studying force in biological systems. AFM force measurements can give insight into protein-protein bond breakage. Such force measurements are possible by taking advantage of the fact that AFM measures deflection from the surface and the force that the tip exerts on the surface. This can then be calibrated to measure the amount of force that the substrate places on the tip. These force measurements were particularly insightful in contextualizing the forces required to shear the SAv bonds to DSB and biotin[32]. These forces gave a valuable starting point for our calculations of whether pipette driven forces were sufficient to shear SAv bonding.

Importance of cell capture and release: We have established optimized conditions to capture and release cells of interest from a multi-cell population, which is an important step towards developing cell isolation paradigms. Cellular separation devices would allow for the quantification of receptor levels[4] from a variety of cell types[55]. Such information can enable the pharmacological or computational modeling that increases efficiency of the targeted treatments[56]; thus, reducing toxicity and even the mortality.

Current isolation limitations: Our system focuses on a secondary anchor targeting release mechanism for the capture and release of cells from a mixed sample. Once functionalized surfaces are developed, the system requires mixing with antibody, surface attachment, and cell removal via biotinylation. We believe that the low number of steps and the gentle approach make it advantageous over some commercially available options. These procedures are personnel limited, thus increasing time, and techniques such as centrifugation may cause the cell to express different markers or proteins than they would physiologically, which when using this technique for disease monitoring may give false information on progression[57]. Thus, new methods are necessary that reduce handling.

Improving cell isolation through biotin-avidin coupling: Our design utilizes DSB-SAv and biotin-SAv interactions, which is commonly used in the biosciences[40,58]. Indeed, the strong, selective binding of the avidin family to the biotin family has been used for over 30 years for a range of scientific and medical applications including: antibody-fluorophore attachment[59] and quantitative Qdot-polystyrene bead attachment[60]. Our utilization of DSB for reversible cell attachment has been similarly used with the Dynabead® system from Life technologies, which

applies DSB-antibodies and magnetic beads for cell separation[61]. However, magnetic isolation can be harsh and result in cellular loss due to the processing steps associated with preparing the samples[62,63]. Additionally, these processing steps can result in differential receptor and chemokine expression[57,63]. Furthermore, the use of the beads adds an additional reagent that our surface functionalization overcomes. Therefore, the approach presented here, offers several improvements over prior technology.

Future improvements: The technology presented here could be further enhanced by using aptamers rather than antibodies, to tailor it for use with other cell types or for specific applications. Future development of molecules that are specific to cell types of interest could be integrated to improve the efficiency of the cell capture using this method. A nano-patterning of the surface could also be tested as another method to improve the efficiency by directing the positions of the ligands. This is important in designing a lab on a chip type of system for sequential separation of different cell types at different stages. Integrating microfluidics with our capture surface to create a separation device is another area that could be further optimized in future versions of the technology. The cell viability may be increased by changing the geometry and flow rate of the device. Previous authors have optimized fluid flow and geometries to increase mixing[18,64–66], while others have optimized materials to reduce the cost of production of the device, allowing for the development of diagnostic devices for personalized medicine[67].

2.5 Conclusion

In summary, novel adhesive ligands combined with creative designs will change the trend of adhesion-based cell sorting devices in the future. There is an immediate need to discover and

introduce cell-specific biomolecules to be used in conjunction with cell separation microfluidic devices. A portable, easy-to-use and inexpensive adhesion-based cell separation microchip can be used in personalized medicine, early stage diagnosis, and in regenerative medicine for separation of tumor cells, stem cells and other rare cell types. This technology would revolutionize personalized medicine and treatment options and improve the physiological relevancy of computational modeling. Additionally, many other applications of this technology can be envisioned for future applications, as this technology can be readily integrated into a variety of existing architectures.

2.6 Figures and Tables

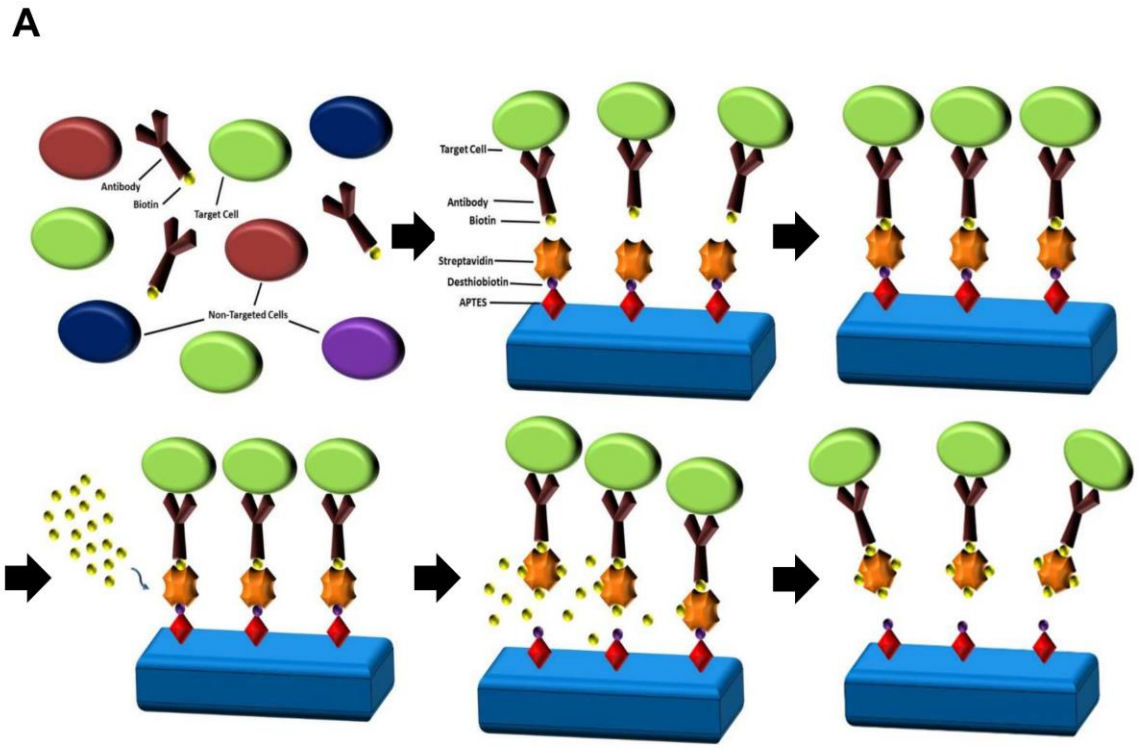

Figure 1. Schematic of surface functionalization for cell isolation. Glass surface functionalized with (3-Aminopropyl) triethoxysilane (APTES), a self-assembling silane that allows for an amine from which subsequent layers can be attached to the glass; DSB which allows for reversible binding to SAv and is the crux of the release mechanism for the cells; SAv which serves as the adaptor that allows for cellular conjugation to the floor; and a cell-specific biotinylated antibody which serves as the differentiation mechanism for the sorting of the cells. The SAv-antibody-cell complex is released via the introduction of excess biotin, which competes with DSB-SAv binding ($K_{d,desthiobiotin\text{-}streptavidin}$= Kd = 10^{-13}, $K_{d,biotin\text{-}streptavidin}$= 10^{-15}). This competition releases the DSB and replaces it with the more strongly bound biotin. This releases the entire cell-antibody-SAv complex from the functionalized surface, allowing for collection.

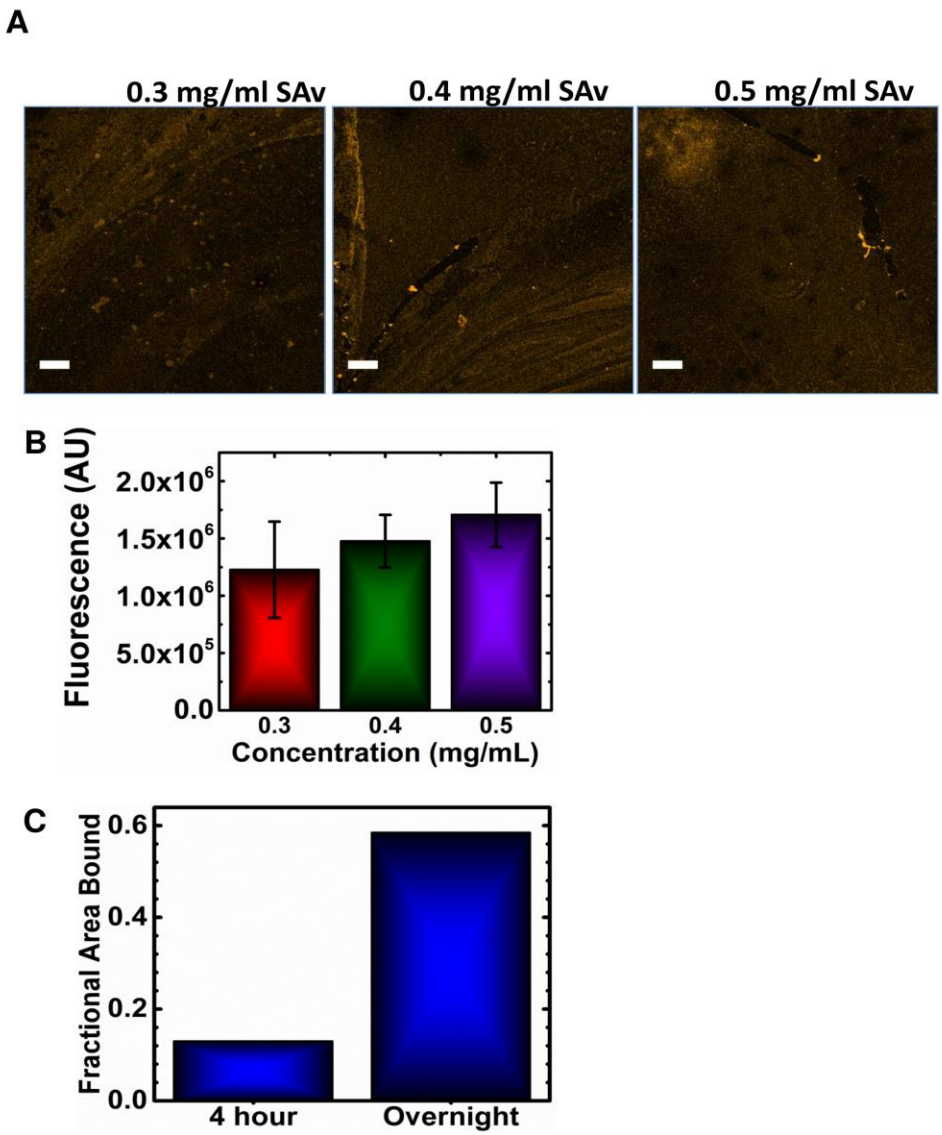

Figure 2. Visualizing capture of Qdots. (A) Surface functionalized with APTES, DSB, and 0.2 mg/mL, 0.3 mg/mL, and 0.4 mg/mL SAv was exposed to excess biotinylated Qdot 605. At .3mg/mL SAv, there are large gaps in the fluorescently labeled areas, which show non-uniformity and incomplete functionalization of SAv. At 0.4 mg/mL, the fluorescence is much more uniform with a mostly complete coating, showing a more complete monolayering of SAv. At 0.5 mg/mL, the entire surface is functionalized non-uniformly resulting in much higher standard deviation in brightness despite more complete coverage, possibly due to multiple layering of SAv. (B) Quantitative graph illustrating the fluorescence profiles. (C) Cells binding to functionalized surfaces incubated with SAv overnight as compared to surfaces incubated with SAv for four hours, showing 4x higher fluorescent activity for overnight incubation.

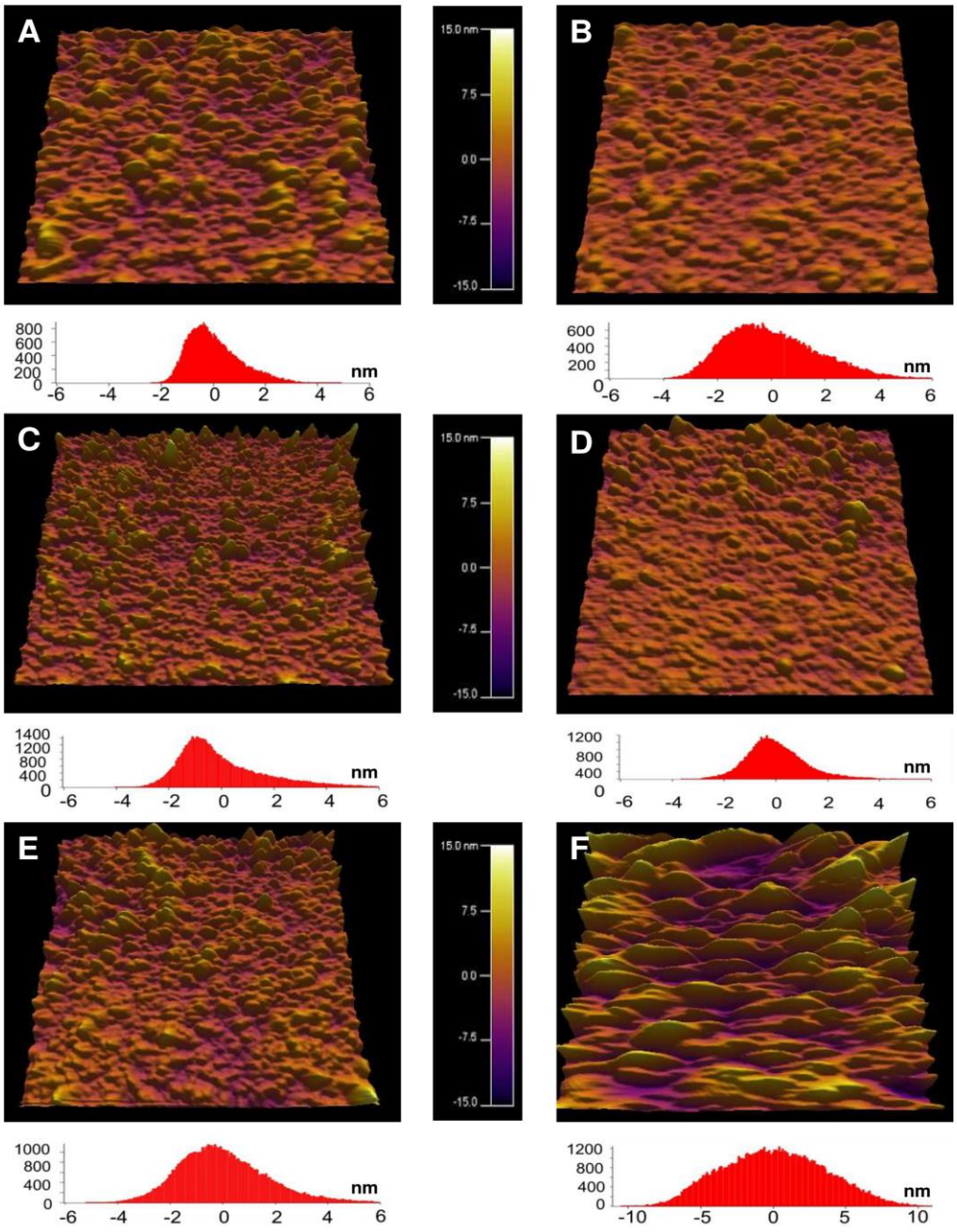

Figure 3. AFM Images of functionalized surfaces and surface height distribution. (A) Ethanol and DI water cleaned glass shows relative heterogeneity on the surface. (B) Oxygen Plasma Cleaned glass (C) Oxygen Plasma Cleaned glass functionalized with 2% APTES, (D) and with 5% APTES show the differences in both the uniformity and the height of the surfaces. (E) Glass functionalized with 2% APTES + DSB and (F) Glass functionalized with 5% APTES + DSB, and SAv show the drastic differences in layering as a result of the changes in the initial APTES layer concentration. The surfaces that have the smaller widths in the distributions are more uniformly distributed. The 5% APTES DSB, and SAv surface has substantially larger a distribution than the other surfaces, and as such has larger bounds than the rest of the surfaces.

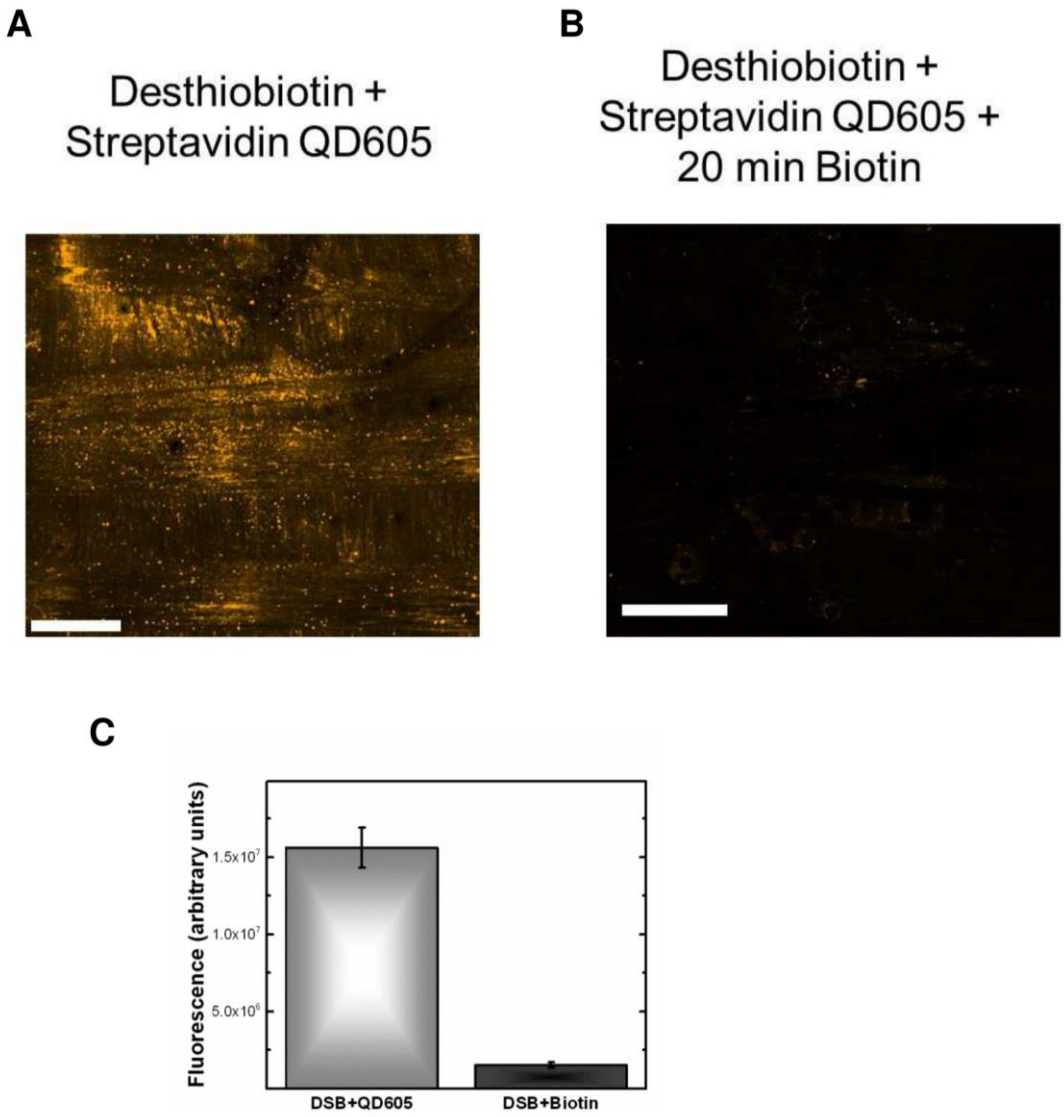

Figure 4. Qdot conjugated biotinylated antibodies on the functionalized surface. (A) Captured 605 Qdots, (B) 605 Qdot release: 20mM biotin solution biotin treatment (C) Comparison of fluorescence showing less fluorescence after application of biotin- showing that the surface has had the functionalized surface removed.

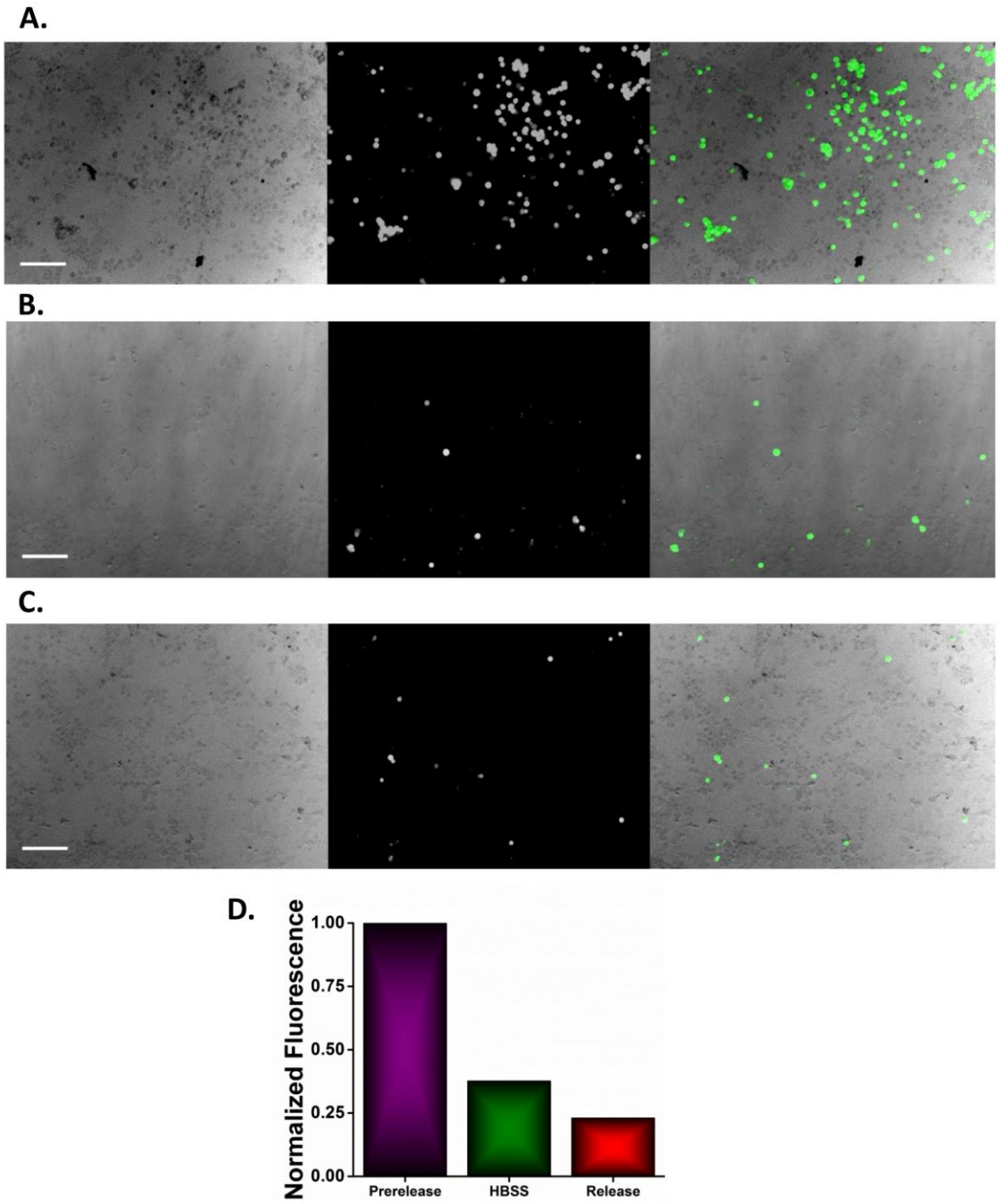

Figure 5. Cellular capture of human breast cancer cells (MCF7-GFP) using hIgG antibody on the fully functionalized surface. (A) Captured cells, (B) Cells remaining after HBSS wash (control), (C) Cells remaining after biotin wash (release), and (D) quantification of capture and release fluorescence showing that the fluorescence is substantially reduced when biotin is introduced, as compared with a HBSS wash.

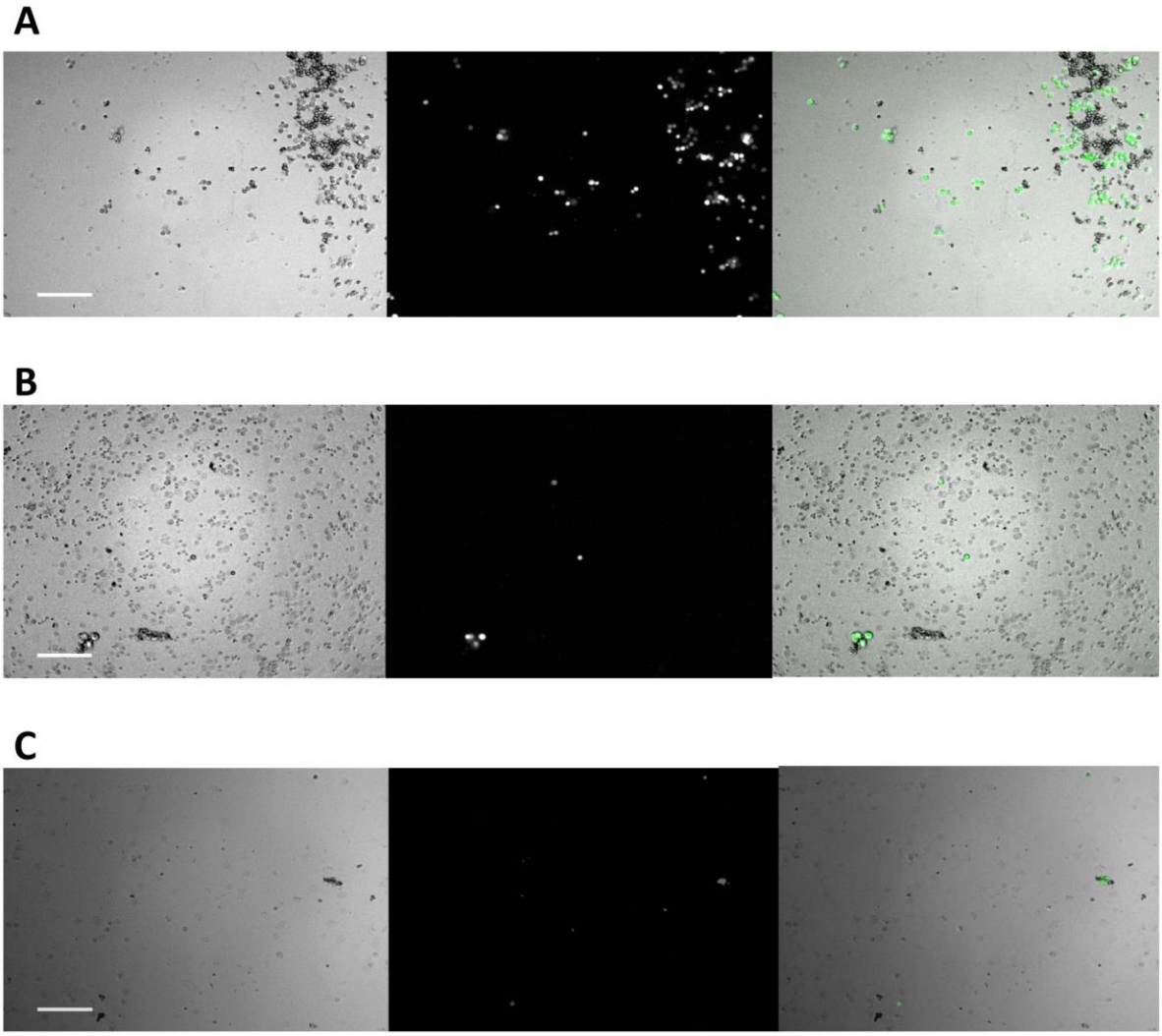

Figure 6. Cellular capture of cellular mixture containing mouse macrophages (RAW 264.7) and human breast cancer cell line (MCF7-GFP). The mCD11b antibody was used to selectively capture macrophages (A) Cells captured onto the surface, (B) cells remaining after HBSS wash (control), (C) cells remaining after biotin wash (release**)**, showing that the RAW macrophages are preferentially captured and that they are released after addition of biotin.

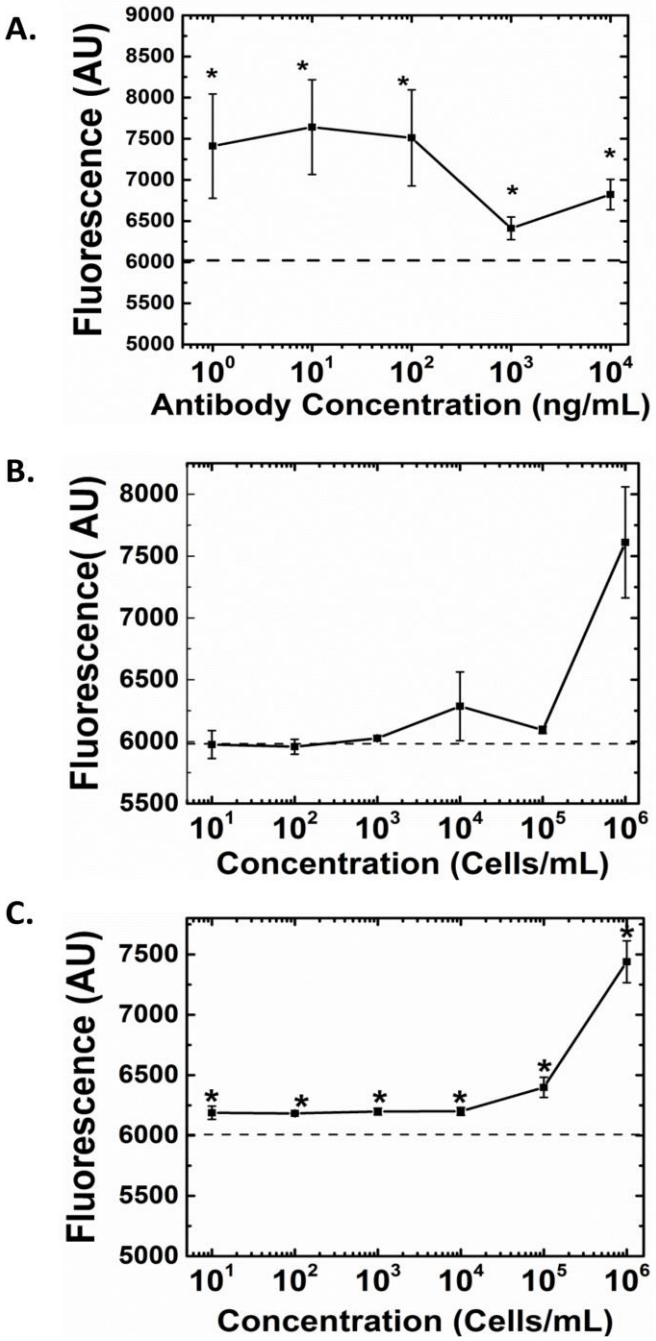

Figure 7. Antibody and Cell Saturation Curves of GFP cells plus antibodies bound to a fully functionalized 24 well plate. Antibody saturation curve of HLA (A) showing that concentrations of 10 ng/mL are ideal. The significance is in comparison to the background, $p < 0.05$. This concentration was used for the cell saturation and titration experiments. Cell concentrations were kept constant at one million cells/mL. Cellular saturation curve using HLA (B) and hIgG (C) antibodies at 10 ng/mL. The blank (background) is shown on the graph as a dashed line.

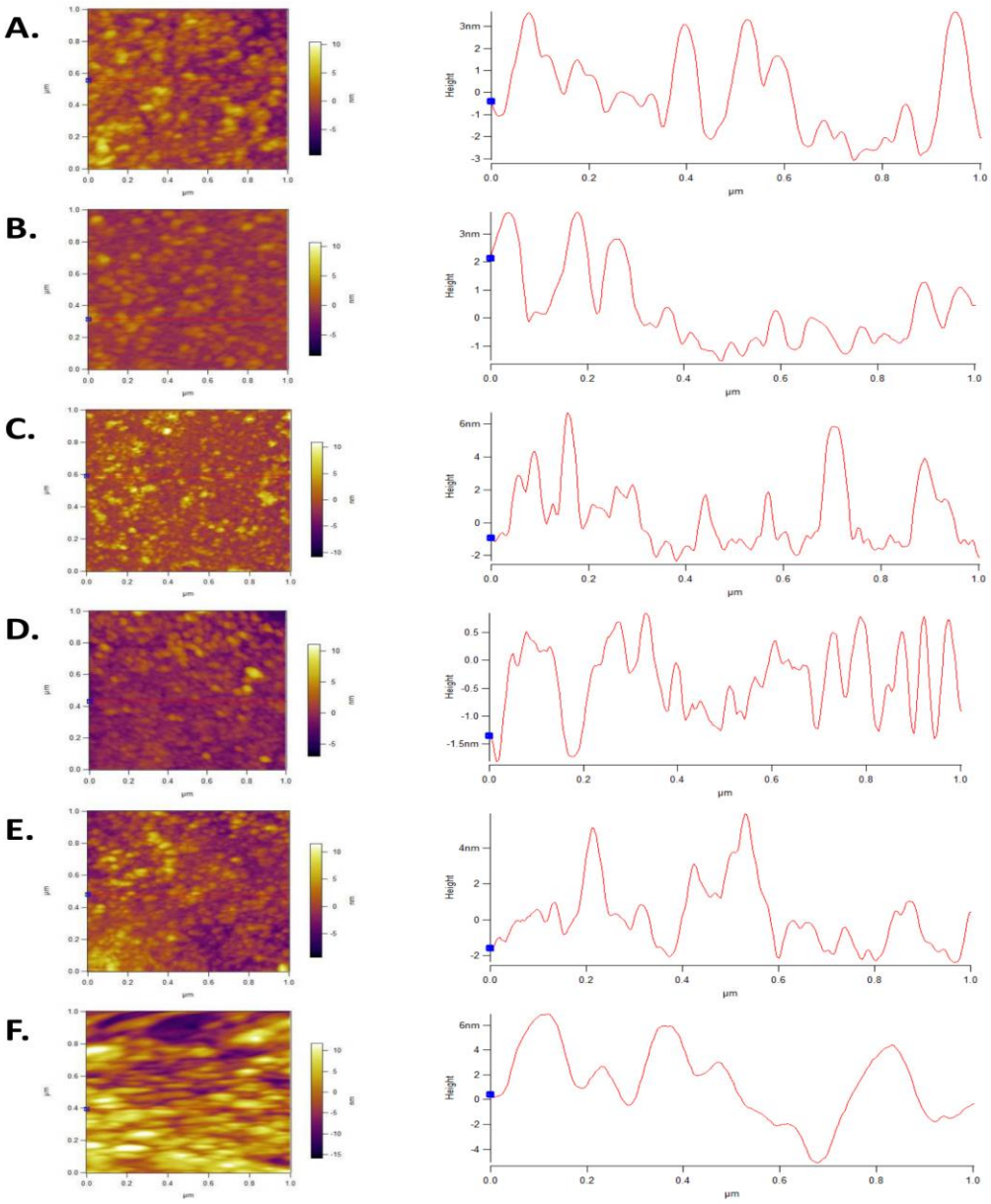

Figure 8. AFM Images of plain, oxygen plasma cleaned, APTES and SAv functionalized glass surfaces with corresponding height measurements. Regular glass cleaned with ethanol and DI water (A) as compared to oxygen plasma cleaned glass (B). The heights shown below correspond to the heights sampled across the red line above. This shows that oxygen plasma cleaned glass is much more uniform than regular glass. 2% APTES functionalized glass (C) as compared to 5% APTES functionalized glass (D). Both glass surfaces were initially oxygen plasma cleaned prior to functionalization. The heights shown below correspond to the heights sampled across the red line above. This shows that 5% APTES seems to be slightly more uniform than 2% APTES. 2% APTES, DSB, and SAv functionalized glass (E) as compared to 5% APTES, DSB, and SAv functionalized glass (F). Both glass surfaces were initially oxygen plasma cleaned prior to functionalization. The heights shown below correspond to the heights sampled across the red line above. This shows that the fully functionalized 2% APTES is much more uniform than the fully functionalized 5% APTES surface.

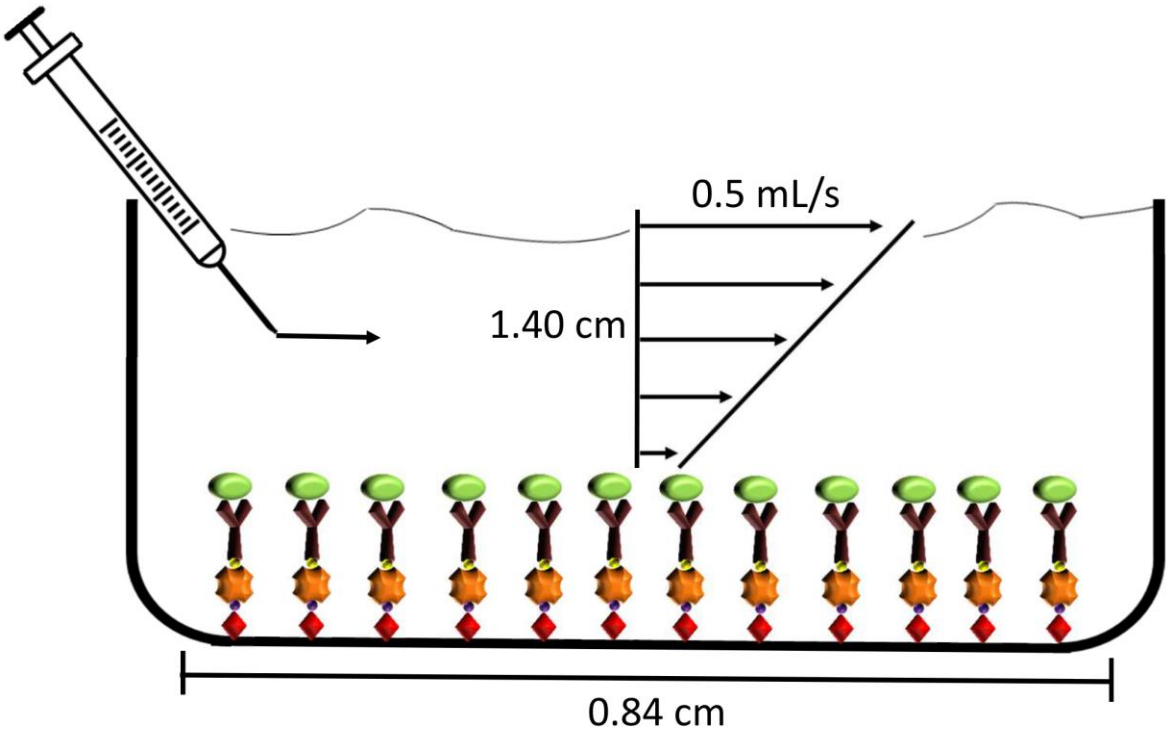

Figure 9 Diagram of shear stress calculation on SAv bonding. Shear stress is calculated assuming that the area is 0.7 cm^2, that the washing step takes 2 seconds, and that there is approximately 1 mL of solution in the well. This shows that the wash steps are insufficient to rupture the SAv bond to either DSB or biotin.

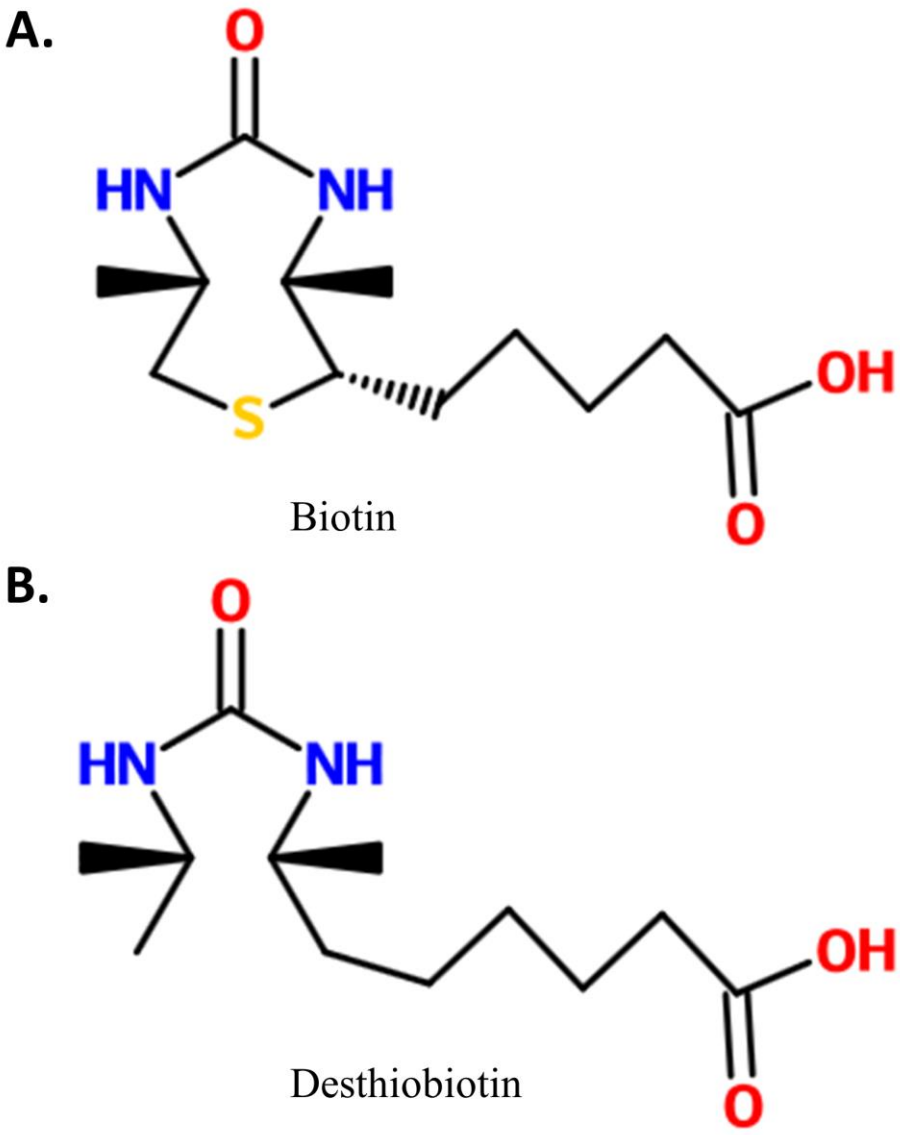

Figure 10. Structural difference between biotin and DSB. Biotin (A) has an additional sulfur group as compared to DSB (B). This result in a difference in structure, which contributes to the lower affinity that DSB has for SAv. All structures were drawn using eMolecules' online drawing tool. (eMolecules, La Jolla, CA).

Table 1. Igor-measured standard deviations of the different functionalized surfaces

Functionalized Surface	Standard Deviation
Glass cleaned with ethanol and DI water	1.969 nm
Glass cleaned with oxygen plasma	1.078 nm
2% APTES functionalized glass	1.419 nm
5% APTES functionalized glass	1.332 nm
2% APTES, DSB, and functionalized glass	2.115 nm
5% APTES, DSB, and SAv functionalized glass	4.951 nm

CHAPTER 3
CUSTOMIZATION AND FUTURE DIRECTIONS

3.1 Customization of the Surface Functionalization for Capture and Release of Cells

The functionalization of the Secondary Anchor Targeted system consists of a binding agent APTES that enables subsequent layering to the glass substrate. Although, the Secondary Anchor Targeted system typically uses glass as the substrate, other surfaces can be functionalized by altering the chemistry slightly to use chemicals other than APTES. For instance, amine-linked thiols could be used in conjunction with gold surfaces to allow for near identical functionalization process and design.

The second layer that is integrated into the Secondary Anchor Targeted Cell Release System is the secondary target itself-desthiobiotin. This serves as the release mechanism and is bound via EDC activation of the desthiobiotin and the amine group of the APTES. This layer can be replaced with other biotin family proteins if needed, but desthiobiotin is used for its substantially lower affinity which is harnessed in the releasing of cells.

The capturing mechanism of the Secondary Anchor Targeted Cell Release System is the streptavidin layer that allows for the pull-down of biotinylated antibody laden cells. When the cells of interest are labeled with the biotinylated antibody, the cells are attracted to the streptavidin, allowing for capture. This layer can also be customized with different avidin family proteins such as Neutravidin or avidin dependent on the functionalization environment. This can

also be substituted with aptamers or other streptavidin mimicking proteins that would provide the suitable binding partner to the biotinylated antibodies.

Overall, the Secondary Anchor Targeted Cell Release system is designed to allow for the gentle capture and release of a targeted cell type from solution. This would allow for cells to be pulled out of solution rapidly, without altering physiological expression- preserving the native information on resistances that a patient may have. Additionally, the surface is able to be customized for any cell type that has a specific antibody target- allowing for probing of several cells of interests for practically any disease of interest.

3.2 Spiral Integration

Glass functionalized by the Secondary Anchor Targeted System can be adapted and integrated in a variety of modalities, allowing for customization and flexibility of medium. We have recently integrated the Secondary Anchor Targeted System into a microfluidic device allowing for the capture and release of cells from a solution in addition to well plates and glass bottom dishes. This adaption is the first of many steps to develop a clinical translation of the device which could help further improve personalized medicine by enriching cellular samples and purifying them without damaging them. We aim to do this by firstly optimizing the capture of cells from the microfluidic device.

We have begun optimizing the microfluidic system by titrating cellular and antibody concentration to find which cells of interest can be captured using specific functionalization protocols. Additionally, we have begun optimizing both flow rate and osmolarity to reduce cellular strain and deformation in the microfluidic device. These changes will improve cell capture and release percentages as we translate to clinical applications.

We then aim to expand the technology to capture cells from blood to allow for capture of rare cell types such as CTC and CECs. We have begun this process through the spiking of endothelial cells in serum and capturing cells from solution. Through calibrating and adapting the functionalization process, we will be able to improve gentle capture from the device.

Lastly, we aim to expand the surface functionalization process to capture cell types beyond the cell types that we have originally tested. This expansion will allow the device to move towards becoming truly clinical. Investigators and clinicians would be able to utilize devices integrated with the Secondary Anchor Targeted Cell System to purify their cells of interest for downstream analysis, personalizing their treatment regimens and reducing toxicities of therapies.

REFERENCES

1. Doroshow, J. H. NCI's Roadmap to Personalized Medicine in Cancer Treatment. in *NCAB 150th Meet.* (2009).
2. Hansen, C. Personalized Medicine: The Future of Cancer Care. *Cancer CANdor* (2015). at <http://www.acscan.org/content/cancer-candor/personalized-medicine-the-future-of-cancer-care/>
3. Salwitz, J. C. The Future is Now: Personalized Medicine. *Expert Voices Blog* (2012). at <http://blogs.cancer.org/expertvoices/2012/04/18/the-future-is-now-personalized-medicine/>
4. Chen, S. *et al.* Current State of the Art and Future Directions in Systems Biology. *Prog. Commun. Sci.*
5. Batchelor, T. T. *et al.* AZD2171, a Pan-VEGF Receptor Tyrosine Kinase Inhibitor, Normalizes Tumor Vasculature and Alleviates Edema in Glioblastoma Patients. *Cancer Cell* **11,** 83–95 (2007).
6. Chen, S. *et al.* QFlow Cytometer-Based Receptoromic Screening: A High-throughput Quantification Approach Informing Biomarker Selection and Nanosensor Development. *Submiss.* (2016).
7. Imoukhuede, P. I. & Popel, A. S. Quantitative fluorescent profiling of VEGFRs reveals tumor cell and endothelial cell heterogeneity in breast cancer xenografts. *Cancer Med.* **3,** 225–44 (2014).
8. Weddell, J. C. & Imoukhuede, P. I. Quantitative characterization of cellular membrane-receptor heterogeneity through statistical and computational modeling.

PLoS One **9,** (2014).

9. Mishra, A., Kwon, J.-S., Thakur, R. & Wereley, S. Optoelectrical microfluidics as a promising tool in biology. *Trends Biotechnol.* **32,** 414–421 (2014).
10. Roxworthy, B. J. *et al.* Plasmonic optical trapping in biologically relevant media. *PLoS One* **9,** e93929 (2014).
11. Cheung, L. S. L. *et al.* Detachment of captured cancer cells under flow acceleration in a bio-functionalized microchannel. *Lab Chip* **9,** 1721–1731 (2009).
12. He, L. *et al.* An automated programmable platform enabling multiplex dynamic stimuli delivery and cellular response monitoring for high-throughput suspension single-cell signaling studies. *Lab Chip* **15,** 1497–1507 (2015).
13. Liu, L., Loutherback, K., Liao, D. & Yeater, D. A microfluidic device for continuous cancer cell culture and passage with hydrodynamic forces. *Lab Chip* **10,** 1807–1813 (2010).
14. Park, K., Akin, D. & Bashir, R. Electrical capture and lysis of vaccinia virus particles using silicon nano-scale probe array. *Biomed. Microdevices* **9,** 877–83 (2007).
15. Plouffe, B. D., Brown, M. a, Iyer, R. K., Radisic, M. & Murthy, S. K. Controlled capture and release of cardiac fibroblasts using peptide-functionalized alginate gels in microfluidic channels. *Lab Chip* **9,** 1507–10 (2009).
16. Sheng, weian, Ogunwobi, O., Chen, T. & Zhang, J. Capture, release and culture of circulating tumor cells from pancreatic cancer patients using an enhanced mixing chip. *Lab Chip* **14,** 89–98 (2014).
17. Galletti, G., Sung, M. & Vahdat, L. Isolation of breast cancer and gastric cancer circulating tumor cells by use of an anti HER2-based microfluidic device. *Lab Chip* **14,**

147–156 (2014).

18. Schudel, B. R., Choi, C. J., Cunningham, B. T. & Kenis, P. J. a. Microfluidic chip for combinatorial mixing and screening of assays. *Lab Chip* **9,** 1676–80 (2009).

19. Lien, K.-Y. *et al.* Rapid isolation and detection of cancer cells by utilizing integrated microfluidic systems. *Lab Chip* **10,** 2875–2886 (2010).

20. Stott, S. L. *et al.* Isolation of circulating tumor cells using a. *PNAS* **107,** 18392–7 (2010).

21. Yu, M., Ting, D., Stott, S., Wittner, B. & Ozsolak, F. RNA sequencing of pancreatic circulating tumour cells implicates WNT signalling in metastasis. *Nature* **487,** 510–513 (2012).

22. Zheng, X., Cheung, L. S.-L., Schroeder, J. A., Jiang, L. & Zohar, Y. A high-performance microsystem for isolating circulating tumor cells. *Lab Chip* **11,** 3269–3276 (2011).

23. Tanzeglock, T., Soos, M., Stephanopoulos, G. & Morbidelli, M. Induction of mammalian cell death by simple shear and extensional flows. *Biotechnol. Bioeng.* **104,** 360–70 (2009).

24. Imoukhuede, P. I. & Popel, A. S. Quantification and cell-to-cell variation of vascular endothelial growth factor receptors. *Exp. Cell Res.* **317,** 955–965 (2011).

25. Imoukhuede, P. I. & Popel, A. S. Expression of VEGF receptors on endothelial cells in mouse skeletal muscle. *PLoS One* **7,** e44791 (2012).

26. Ludwig, a, Kretzmer, G. & Schügerl, K. Determination of a 'critical shear stress level' applied to adherent mammalian cells. *Enzyme Microb. Technol.* **14,** 209–13 (1992).

27. Hoffmann, M. *et al.* Molecular recognition in biotin-streptavidin systems and analogues at the air-water interface. *Thin Solid Films* **210-211,** 780–783 (1992).

28. Magalhães, M. L. B. *et al.* Evolved streptavidin mutants reveal key role of loop residue in high-affinity binding. *Protein Sci.* **20,** 1145–54 (2011).

29. Qureshi, M. H. & Wong, S.-L. Design, production, and characterization of a monomeric streptavidin and its application for affinity purification of biotinylated proteins. *Protein Expr. Purif.* **25,** 409–415 (2002).

30. Caicedo, H. M., Dempere, L. a & Vermerris, W. Template-mediated synthesis and bio-functionalization of flexible lignin-based nanotubes and nanowires. *Nanotechnology* **23,** 105605 (2012).

31. Kuzuya, A., Numajiri, K., Kimura, M. & Komiyama, M. Single-molecule accommodation of streptavidin in nanometer-scale wells formed in DNA nanostructures. *Nucleic Acids Symp. Ser. (Oxf).* 681–682 (2008). doi:10.1093/nass/nrn344

32. Lee, C. K., Wang, Y. M., Huang, L. S. & Lin, S. Atomic force microscopy: Determination of unbinding force, off rate and energy barrier for protein-ligand interaction. *Micron* **38,** 446–461 (2007).

33. Mantovani, A., Sozzani, S., Locati, M., Allavena, P. & Sica, A. Macrophage polarization: tumor-associated macrophages as a paradigm for polarized M2 mononuclear phagocytes. *Trends Immunol.* **23,** 549–55 (2002).

34. Murdoch, C., Giannoudis, A. & Lewis, C. E. Mechanisms regulating the recruitment of macrophages into hypoxic areas of tumors and other ischemic tissues. *Blood* **104,** 2224–34 (2004).

35. Drews-Elger, K. *et al.* Primary breast tumor-derived cellular models: characterization of tumorigenic, metastatic, and cancer-associated fibroblasts in dissociated tumor (DT) cultures. *Breast Cancer Res. Treat.* **144,** 503–17 (2014).

36. Drenan, R. M. *et al.* Subcellular trafficking, pentameric assembly, and subunit stoichiometry of neuronal nicotinic acetylcholine receptors containing fluorescently labeled alpha6 and beta3 subunits. *Mol. Pharmacol.* **73,** 27–41 (2008).

37. Imoukhuede, P. I., Dokun, A. O., Annex, B. H. & Popel, A. S. Endothelial cell-by-cell profiling reveals the temporal dynamics of VEGFR1 and VEGFR2 membrane localization after murine hindlimb ischemia. *Am. J. Physiol. Heart Circ. Physiol.* **304,** H1085–93 (2013).

38. Bashir, R. *et al.* Adsorption of avidin on microfabricated surfaces for protein biochip applications. *Biotechnol. Bioeng.* **73,** 324–8 (2001).

39. Esseghaier, C. *et al.* Impedance spectroscopy on immobilized streptavidin horseradish peroxidase layer for biosensing. *Sensors Actuators B Chem.* **134,** 112–116 (2008).

40. Hirsch, J. D. *et al.* Easily reversible desthiobiotin binding to streptavidin, avidin, and other biotin-binding proteins: uses for protein labeling, detection, and isolation. *Anal. Biochem.* **308,** 343–357 (2002).

41. Holmberg, A. *et al.* The biotin-streptavidin interaction can be reversibly broken using water at elevated temperatures. *Electrophoresis* **26,** 501–510 (2005).

42. Lagunas, A., Comelles, J., Martínez, E., Samitier, J. & Martínez, E. Universal Chemical Gradient Platforms Using Poly(methyl methacrylate) Based on the Biotin–Streptavidin Interaction for Biological Applications. *Langmuir* **26,** 14154–14161 (2010).

43. Nelson, K. E. *et al.* Surface Characterization of Mixed Self-Assembled Monolayers Designed for Streptavidin Immobilization. *Langmuir* **17,** 2807–2816 (2001).

44. Su, X., Wu, Y.-J., Robelek, R. & Knoll, W. Surface plasmon resonance spectroscopy and quartz crystal microbalance study of streptavidin film structure effects on biotinylated DNA assembly and target DNA hybridization. *Langmuir* **21,** 348–53 (2005).

45. Butt, H. J., Cappella, B. & Kappl, M. Force measurements with the atomic force microscope: Technique, interpretation and applications. *Surf. Sci. Rep.* **59,** 1–152 (2005).

46. Cappella, B. & Dietler, G. Force-distance curves by atomic force microscopy. *Surf. Sci. Rep.* **34,** 1–104 (1999).

47. Lee, G. U., Kidwell, D. a & Colton, R. J. Sensing Discrete Streptavidin-Biotin Interactions with Atomic Force Microscopy. *Langmuir* **2,** 354–357 (1994).

48. Willemsen, O. H. *et al.* Biomolecular interactions measured by atomic force microscopy. *Biophys. J.* **79,** 3267–3281 (2000).

49. Williams, E. H. *et al.* Immobilization of streptavidin on 4H-SiC for biosensor development. *Appl. Surf. Sci.* **258,** 6056–6063 (2012).

50. D'Antò, V. *et al.* Evaluation of surface roughness of orthodontic wires by means of atomic force microscopy. *Angle Orthod.* **82,** 922–928 (2012).

51. Chen, Y. & Huang, W. Numerical simulation of the geometrical factors affecting surface roughness measurements by AFM. *Meas. Sci. Technol.* **15,** 2005–2010 (2004).

52. Boussu, K. *et al.* Roughness and hydrophobicity studies of nanofiltration membranes using different modes of AFM. *J. Colloid Interface Sci.* **286,** 632–638 (2005).

53. El Feninat, F., Elouatik, S., Ellis, T. H., Sacher, E. & Stangel, I. Quantitative assessment of surface roughness as measured by AFM: Application to polished human dentin.

Appl. Surf. Sci. **183,** 205–215 (2001).

54. Jalili, N. & Laxminarayana, K. A review of atomic force microscopy imaging systems: Application to molecular metrology and biological sciences. *Mechatronics* **14,** 907–945 (2004).

55. Yu, M., Stott, S., Toner, M., Maheswaran, S. & Haber, D. A. Circulating tumor cells: approaches to isolation and characterization. *J. Cell Biol.* **192,** 373–382 (2011).

56. Chen, S., Guo, X., Imarenezor, O. & Imoukhuede, P. I. Quantification of VEGFRs, NRP1, and PDGFRs on Endothelial Cells and Fibroblasts Reveals Serum, Intra-Family Ligand, and Cross-Family Ligand Regulation. *Cell. Mol. Bioeng.* **8,** 383–403 (2015).

57. Naranbhai, V. *et al.* Impact of blood processing variations on natural killer cell frequency, activation, chemokine receptor expression and function. *J. Immunol. Methods* **366,** 28–35 (2011).

58. Wilchek, M. & Bayer, E. A. Applications of Avidin-Biotin Technology: Literature Survey. *Methods Enzymol.* **152,** 183–189 (1987).

59. Wu, G. *et al.* Hypoxia induces myocyte-dependent COX-2 regulation in endothelial cells: role of VEGF. *Am. J. Physiol. Heart Circ. Physiol.* **285,** H2420–9 (2003).

60. Lee-Montiel, F. T. & Imoukhuede, P. I. Engineering quantum dot calibration standards for quantitative fluorescent profiling. *J. Mater. Chem. B* **1,** 6434 (2013).

61. Hornes, E. & Korsnes, L. Oligonucleotide-linked magnetic particles and uses thereof. (1996). at <http://www.google.com/patents/US5512439>

62. Allard, W. J. *et al.* Tumor Cells Circulate in the Peripheral Blood of All Major Carcinomas but not in Healthy Subjects or Patients With Nonmalignant Diseases Tumor Cells Circulate in the Peripheral Blood of All Major Carcinomas but not in

Healthy Subjects or Patients With Non. **10,** 6897–6904 (2005).

63. Nagrath, S. *et al.* Isolation of rare circulating tumour cells in cancer patients by microchip technology. *Nature* **450,** 1235–9 (2007).

64. Winkler, C. M., Rani, S. L. & Vanka, S. P. Preferential concentration of particles in a fully developed turbulent square duct flow. *Int. J. Multiph. Flow* **30,** 27–50 (2004).

65. Watkins, N. N. *et al.* Microfluidic CD4+ and CD8+ T lymphocyte counters for point-of-care HIV diagnostics using whole blood. *Sci. Transl. Med.* **5,** 214ra170 (2013).

66. Gabrielson, N. P. *et al.* Cell-laden hydrogels in integrated microfluidic devices for long-term cell culture and tubulogenesis assays. *Small* **9,** 3076–81 (2013).

67. Luecha, J., Hsiao, A., Brodsky, S., Liu, G. L. & Kokini, J. L. Green microfluidic devices made of corn proteins. *Lab Chip* **11,** 3419–25 (2011).

68. Bergers, G. & Hanahan, D. Modes of resistance to anti-angiogenic therapy. *Nat Rev Cancer* **8,** 592–603 (2008).

69. Ramos, P. & Bentires-Alj, M. Mechanism-based cancer therapy: resistance to therapy, therapy for resistance. *Oncogene* 1–10 (2014). doi:10.1038/onc.2014.314

70. Wyatt Shields IV, C., Reyes, C. D. & López, G. P. Microfluidic cell sorting: a review of the advances in the separation of cells from debulking to rare cell isolation. *Lab Chip* **15,** 1230–1249 (2015).

71. Wynick, D. & Bloom, S. Magnetic bead separation of anterior pituitary cells. *Neuroendocrinology* (1990). at <http://scholar.google.com/scholar?hl=en&btnG=Search&q=intitle:No+Title#0>

72. Imoukhuede, P. I., Dokun, A. O., Annex, B. H. & Popel, A. S. Endothelial cell-by-cell profiling reveals temporal dynamics of VEGFR1 and VEGFR2 membrane-localization

following murine hindlimb ischemia. *Am J Physiol Hear. Circ Physiol* **4,** H1085–93 (2013).

73. Dittrich, P. S. & Manz, A. Lab-on-a-chip: microfluidics in drug discovery. *Nat Rev Drug Discov* **5,** 210–218 (2006).